Boosting Oxygen Reduction Reaction Activity of Palladium by Stabilizing Its Unusual Oxidation States in Perovskite

ARTICLE *in* CHEMISTRY OF MATERIALS · APRIL 2015

Impact Factor: 8.35 · DOI: 10.1021/acs.chemmater.5b00450

CHEMISTRY OF MATERIALS

Article

pubs.acs.org/cm

Boosting Oxygen Reduction Reaction Activity of Palladium by Stabilizing Its Unusual Oxidation States in Perovskite

Yinlong Zhu,[†] Wei Zhou,*[,†] Yubo Chen,[†] Jie Yu,[†] Xiaomin Xu,[†] Chao Su,[‡] Moses O. Tadé,[‡] and Zongping Shao*[,‡,§]

[†]State Key Laboratory of Materials-Oriented Chemical Engineering, College of Chemistry & Chemical Engineering, Nanjing Tech University, No. 5 Xin Mofan Road, Nanjing 210009, P.R. China

[‡]Department of Chemical Engineering, Curtin University, Perth, Western Australia 6845, Australia

[§]State Key Laboratory of Materials-Oriented Chemical Engineering, College of Energy, Nanjing Tech University, No. 5 Xin Mofan Road, Nanjing 210009, P.R. China

Supporting Information

ABSTRACT: The high cost, scarcity, and poor stability of metallic platinum (Pt) as an oxygen reduction reaction (ORR) catalyst in fuel cells and metal-air batteries have limited the commercialization of these attractive clean-energy technologies. Thus, developing alternative electrocatalysts that are economical and achieve maximized efficiency of stably catalyzing ORR is of prime importance in the societal pursuit of sustainable energy. Metallic palladium (Pd) is an alternative electrocatalyst that is less expensive than Pt; however, its current performance remains insufficient. Here we report for the first time that the ORR activity of the different oxidation states of Pd increased in the following order: Pd^0 < Pd^{2+} < perovskite-type ionic (Pi) $Pd^{3/4+}$. Especially, the intrinsic activity on Pd active site of (Pi) $Pd^{3/4+}$ is ~84-fold higher than that of Pd^0. By doping the Pd element as a cation into the perovskite oxide lattice to form $LaFe_{0.95}Pd_{0.05}O_{3-\delta}$ and $LaFe_{0.9}Pd_{0.1}O_{3-\delta}$, unusual oxidation states of 3/4+ for Pd are stabilized, and the catalysts exhibit superior mass activity, durability, and tolerance to methanol compared with the benchmark commercial Pt/C catalyst.

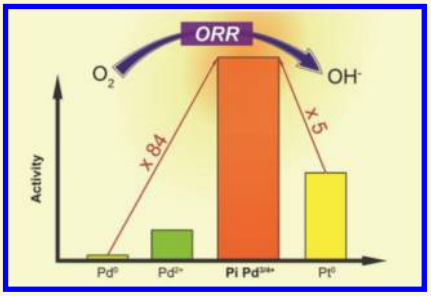

1. INTRODUCTION

The oxygen reduction reaction (ORR) plays a critical role in many energy storage and conversion systems, such as fuel cells, metal-air batteries, and chlor-alkali electrolysis.[1−3] Currently, metallic platinum (Pt) and Pt-based alloys are recognized as the most popular and efficient electrocatalysts for ORR.[4,5] However, the high cost, limited resources, low stability, and vulnerability to fuel (e.g., methanol)-poisoning effects have severely hindered the large-scale applications of Pt in the mentioned fields.[6,7] Therefore, the development of Pt-free electrocatalysts for ORR with improved catalytic activity and durability is highly desirable but remains a significant challenge.

As a potential replacement for the Pt electrocatalyst for ORR, palladium (Pd) has received considerable attention because its physical properties are similar to those of Pt, including a face-centered cubic (fcc) crystal structure, a similar atomic size and electronic configuration.[8] In addition, Pd is less inexpensive and more abundant than Pt.[9,10] Extensive studies on Pd as an ORR electrocatalyst have achieved substantial advancements, such as the synthesis of stable amorphous Pd nanoparticles,[11,12] the ability to manipulate the size, shape, and crystal facets of Pd nanoparticles,[13−15] the combination of Pd with other metals to yield bimetallic catalysts,[16,17] and the use of various support materials to improve the catalytic activity and stability of Pd.[18,19] Unfortunately, in many cases, the current performance of metallic Pd remains significantly inferior to Pt.[10] Significant advances are still required for the use of Pd as a practical ORR electrocatalyst. Recently, Suntivich et al. demonstrated that the ORR activity of many perovskite oxides are closely related to the occupancy of the antibonding orbital, which is dependent on the oxidation state of the B-site cation and the spin state of the electrons.[20] This result indicates that the catalytic activity of a catalyst for ORR may be tailored by tuning the oxidation state of its active element. However, very little information is available about the effect of the oxidation state of Pd on ORR activity, likely due to the difficulty in manipulating the oxidation state to a higher level for Pd (e.g., 3/4+).

Here we report that significant improvement in the ORR activity of Pd can be achieved by stabilizing its unusual high oxidation states via doping the element into a perovskite oxide lattice. More specifically, by synthesis and further post-treatment of a Pd-containing $LaFe_{0.95}Pd_{0.05}O_3$ (LFP0.05) perovskite oxide, a well-known automotive emission catalyst,[21] different Pd species with 0, 2+, or unusual 3/4+ oxidation states were successfully created. The electrochemical studies showed that the ORR activity of the different oxidation states of Pd increased in the following order: Pd^0 < Pd^{2+} < perovskite-type ionic (Pi) $Pd^{3/4+}$. Especially, the intrinsic activity of (Pi) $Pd^{3/4+}$

Received: February 5, 2015
Revised: March 21, 2015
Published: April 5, 2015

DOI: 10.1021/acs.chemmater.5b00450
Chem. Mater. 2015, 27, 3048−3054

was ~84-fold higher than that of Pd^0. Moreover, the $LaFe_{1-x}Pd_xO_{3-\delta}$ (LFP, x = 0.05 and 0.1) perovskite (containing Pi $Pd^{3/4+}$) exhibited a ~2.5-fold higher ORR mass activity than the benchmark Pt/C catalyst based on the mass of the Pd or Pt noble metal, together with a superior durability and immunity to methanol. The optimal e_g orbital filling (e_g = 1) and the downshift of the d-band center of Pi $Pd^{3/4+}$ possibly contribute to the unusually high ORR activity. Keeping costs low and maximizing the efficiency of stably catalyzing ORR through the use of perovskite-type ionic noble metal (e.g., $Pd^{3/4+}$) catalysts provides a potential solution to the problem of the noble metal (e.g., Pd) abundance and stability as ORR electrocatalysts, which could be a major contribution to the sustainable energy demands of our society.

2. EXPERIMENTAL SECTION

Catalyst Synthesis and Thermal Treatment. The perovskite oxides, namely $LaFeO_3$ (LF), $LaFe_{0.95}Pd_{0.05}O_3$ (LFP0.05), and $LaFe_{0.9}Pd_{0.1}O_3$ (LFP0.1) were synthesized by a standard combined EDTA−citrate complexing sol−gel process. Stoichiometric amounts of $La(NO_3)_3{\cdot}6H_2O$, $Fe(NO_3)_3{\cdot}9H_2O$ for LF, $La(NO_3)_3{\cdot}6H_2O$, $Fe(NO_3)_3{\cdot}9H_2O$, $Pd(NO_3)_2{\cdot}2H_2O$ (all analytical grade, Sinopharm Chemical Reagent Co., Ltd.) for LFP0.05 and LFP0.1, were mixed in deionized water. EDTA and citric acid were then added as complexing agents in sequence at a mole ratio of 1:1:2 for total metal ions: EDTA:citric acid. To ensure complete complexation, the pH of the solution was adjusted to ~6 by the addition of an NH_3 aqueous solution. A transparent gel was obtained by heating at 90 °C under stirring. The gel was then heated in the furnace for 5 h at 250 °C in air to form a solid precursor. Finally, the solid precursors of LF, LFP0.05, and LFP0.1 were all calcined in air at 800 °C for 5 h. The commercial 20 wt % Pt/C catalyst in this study was purchased from the Johnson Matthey Company. Then, the prepared LFP0.05 perovskite oxide was thermally treated under a reductive or oxidative atmosphere. LFP0.05 was reduced in an atmosphere of 10% H_2/90% Ar at 800 °C for 1 h (denoted as LFP0.05-R). Then, LFP0.05-R was reoxidized in air at 400 °C for 1 h (denoted as LFP0.05-RO).

Basic Characterization. The prepared catalysts were characterized by room temperature (RT) powder diffraction for phase identification and to evaluate the phase purity. A diffractometer (Rigaku Smartlab, Cu Kα radiation, λ = 1.5418 Å) in Bragg−Brentano reflection geometry was used. The diffraction patterns were recorded by continuous scanning in the 2θ range of 20−90° with an interval of 0.02°. The obtained diffraction profiles were analyzed by the Rietveld method with the GSAS program and the EXPGUI interface. During the refinement, the scale factor, lattice parameters, peak shape (pseudo-Voigt function), background, and isotropic atomic displacement parameters were refined. The surface element states were determined by X-ray photoelectron spectroscopy (XPS, PHI5000 VersaProbe spectrometer equipped with an Al Kα X-ray source). High-resolution transmission electron microscopy (HRTEM) was conducted at 200 kV with a Philips Tecnai T30F field emission instrument equipped with a 2k-CCD camera. High-angle annular dark-field scanning TEM (HAADF-STEM) and energy dispersive X-ray (EDX) analyses were conducted on a Cs-corrected STEM (TitanG2 80−200 ChemiSTEM equipped with a Super-X EDX detector system). The morphologies of the catalysts were observed using an environmental scanning electron microscope (ESEM, QUANTA-2000).

Electrochemical Measurements. The electrochemical measurements were performed at room temperature using a rotating disk electrode (RDE) made of glassy carbon (PINE, 5 mm diameter, 0.196 cm^2) connected to a PARSTAT 2273 (Princeton Applied Research) advanced electrochemical system. The glassy carbon (GC) electrode was prepolished with 50 nm α-Al_2O_3 slurries on a polishing cloth and sonicated in ethanol for 5 min. The electrodes were finally rinsed with deionized water and dried before each test. A Pt foil and Ag/AgCl (3.5 M KCl) were used as the counter and reference electrodes, respectively. The preparation method of the working electrodes containing the investigated catalysts is stated as follows: to remove any electrode conductivity limitations present in the thin film electrodes, the perovskite catalysts were mixed with as-received conductive carbon (Super P Li) at a mass ratio of 1:1. Briefly, the electrocatalyst suspensions were prepared by sonication of a mixture of oxide (10 mg), conductive carbon (10 mg), Nafion solution (5 wt %, 100 μL), and ethanol (1 mL) for at least 1 h to generate a homogeneous ink. Next, a 5 μL aliquot of the as-prepared catalyst ink was pipetted on the surface of the GC electrode, yielding an approximate catalyst loading of 0.464 mg_{total} cm^{-2} (0.232 mg_{cat} cm^{-2}) and dried at ambient. The commercial 20 wt % Pt/C catalyst was also measured for comparison. The working electrodes were prepared as follows: 5 mg of Pt/C and 100 μL of Nafion solution (5 wt %) were dispersed in 1 mL of ethanol by sonication for at least 1 h to obtain a well-dispersed ink. Then, a 5 μL aliquot of catalyst ink was pipetted on the surface of the GC electrode, leading to an approximate catalyst loading of 0.116 mg_{total} cm^{-2} (23.2 μg_{Pt} cm^{-2}) and dried at ambient.

The electrolyte was a 0.1 M KOH aqueous solution, which was saturated with O_2 for ~30 min prior to each test and maintained under O_2 atmosphere throughout the experiment. Cyclic voltammetry (CV) curves of the perovskite catalysts were recorded in an O_2-saturated 0.1 M KOH solution at a scan rate of 100 mV s^{-1} between 0.2 and −0.6 V versus Ag|AgCl (3.5 M KCl). Linear sweeping voltammetry (LSV) curves of the perovskite catalysts were recorded by using RDE at different rotation speeds (2500, 2000, 1600, 1200, 800, 400 rpm) in an O_2-saturated 0.1 M KOH solution at a scan rate of 5 mV s^{-1} from 0.2 to −0.6 V (negative scan) versus Ag|AgCl (3.5 M KCl). Notably, the LSVs of the commercial 20 wt % Pt/C catalyst were recorded in the positive scan (−0.6 to 0.2 V) to avoid performance loss caused by anion adsorption. The accelerated stability tests were performed in O_2-saturated 0.1 M KOH at 1600 rpm by potential cycling between 0.2 and −0.6 V versus Ag/AgCl (3.5 M KCl) at a scan rate of 100 mV/s for 1000 cycles.

The kinetic parameters, such as electron transfer number and kinetic current density, can be determined from the following Koutecky−Levich (K−L) equation:

$$\frac{1}{J} = \frac{1}{J_K} + \frac{1}{J_L} = \frac{1}{nFkC^0} + \frac{1}{0.62nFD_{o_2}^{2/3}\nu^{-1/6}C^0\omega^{1/2}} \quad (1)$$

where J corresponds to the measured current density, J_k and J_L are the kinetic and diffusion-limiting current densities, respectively, n is the electron transfer number, F is the Faraday constant, $C°$ is the saturated concentration of oxygen in 0.1 M KOH, ω is the rotating rate (rad s^{-1}), D_{O_2} is the diffusion coefficient of oxygen, ν is the kinetic viscosity of the solution, and k is the rate constant for oxygen reduction. Notably, the J_k at −0.6 V versus Ag/AgCl (3.5 M KCl) can be regarded as the kinetic-limiting current densities. To construct the Tafel curve, the kinetic current was calculated using mass-transport correction $[J_k = (J_L \times J)/(J_L - J)]$. J_k is independent of ω; thus, in the $1/J_{limit}$ $-1/\omega^{1/2}$ plot, the slope is $1/B$, where J_{limit} is the limit measured current density at −0.6 V (vs Ag/AgCl) at each ω. The B factor can be applied to obtain J_L in the ORR.

3. RESULTS AND DISCUSSION

Catalyst Synthesis and Thermal Treatment. The perovskite oxides, namely Pd-free $LaFeO_{3-\delta}$ (LF) and two Pd-containing $LaFe_{1-x}Pd_xO_{3-\delta}$ (LFP, x = 0.05 and 0.1) compounds, were synthesized by a standard combined EDTA−citrate complexing sol−gel process.[22] The $LaFe_{0.95}Pd_{0.05}O_{3-\delta}$ and $LaFe_{0.9}Pd_{0.1}O_{3-\delta}$ perovskite oxides are denoted as LFP0.05 and LFP0.1, respectively. The synthesis details are provided in the Experimental Section. To obtain Pd catalysts with different oxidation states, LFP0.05 perovskite oxide was thermally treated under a reductive atmosphere or further thermally treated under an oxidative atmosphere. LFP0.05 treated in an atmosphere of 10% H_2/90% Ar at 800

DOI: 10.1021/acs.chemmater.5b00450
Chem. Mater. 2015, 27, 3048−3054

°C for 1 h is denoted as LFP0.05-R, while the product from the reoxidization of LFP0.05-R in air at 400 °C for 1 h is denoted as LFP0.05-RO.

Catalyst Characterization. The phase structure of LFP0.05 was initially analyzed by X-ray diffraction (XRD) with the typical pattern presented in Figure 1a. Rietveld

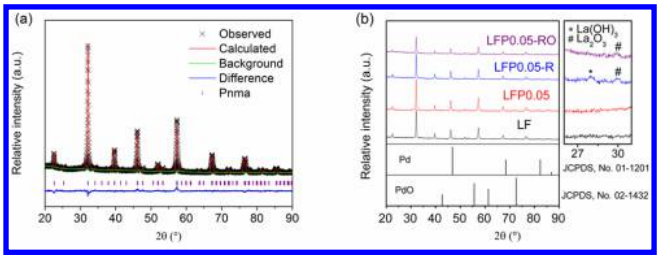

Figure 1. (a) Refined X-ray diffraction profiles of the LFP0.05. (b) X-ray diffraction profiles of LF, LFP0.05, LFP0.05-R, and LFP0.05-RO, with an expanded region of 2θ = 26−31° shown on the right.

refinement revealed that the LFP0.05 possessed an orthorhombic structure with lattice parameters of a = 5.57(1) Å, b = 7.86(1) Å, c = 5.56(4) Å and a space group of *Pnma*.[23,24] The reliability of the Rietveld refinement is R_p = 2.69%, R_{wp} = 3.38%, and χ^2 = 1.81, which is satisfactory regarding the goodness of fit. The phase structure of LFP0.05 was further confirmed by the high-resolution (HR) TEM (the d spacing value of 0.787 nm for [010] zone axes) and the corresponding fast Fourier transform (FFT) images (Figure 2, panels a and b). Figure 1b shows the XRD patterns of LF, LFP0.05, LFP0.05-R, and LFP0.05-RO. A perovskite-type orthorhombic crystal structure can be clearly observed in all of the samples. In addition, after the reduction−oxidation treatment, La_2O_3/$La(OH)_3$ can be found in small quantities (~5 wt % estimated from a quantitative Rietveld refinement) as a secondary phase in LFP0.05-R and LFP0.05-RO. In order to keep the mole ratio of A- and B-site atoms at unit in perovskite to maintain its ABO_3 molecular formula, certain amount of La_2O_3 was also segregated out from the A-site of the LFP0.05 to balance the segregated Pd from B-site. $La(OH)_3$ is originating from the reaction of La_2O_3 with H_2O in air. However, no metallic Pd or PdO diffraction peaks were observed, which may be attributed to the fine dispersion and the small size of these particles.[21,25]

To verify above consideration, the morphologies and compositions of the LFP0.05-R and LFP0.05-RO catalysts were characterized with the results shown in Figure 2 (panels c−h). A high-angle annular dark field scanning transmission electron microscopy (HAADF-STEM) image of LFP0.05-R (Figure 2c) clearly revealed that some nanosized metallic Pd particles (6−8 nm) were homogeneously dispersed on the surface of the catalyst. The phenomenon was further confirmed by the energy-dispersive X-ray spectroscopy (EDX) elemental mapping (Figure 2d) and compositional line profiles (Figure 2e) obtained from a magnified image. EDX mapping and the compositional line profiles revealed that Pd was separated out onto the catalyst surface from the B-site of the LFP0.05 perovskite lattice after the reduction treatment. Similarly, some nanosized PdO particles (8−10 nm) were homogeneously supported on the catalyst surface from the HAADF-STEM image of LFP0.05-RO (Figure 2f), which was clearly demonstrated in the EDX spectra measured from two different positions (P1 and M1) (Figure 2, panels g and h). Notably, the Cu and C peaks of the EDX spectra emanated from the carbon-

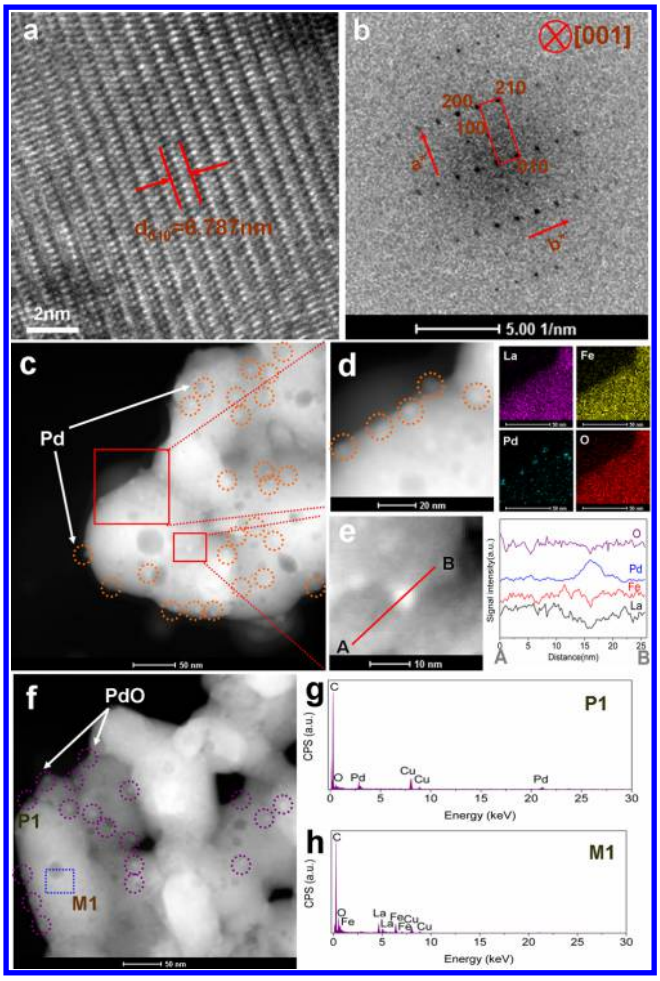

Figure 2. (a and b) The HRTEM and corresponding fast Fourier transform (FFT) images of the [100] zone axes for LFP0.05. (c) HAADF- STEM images of LFP0.05-R. The orange circles in (c) mark some of Pd particles. (d) A magnified image of the section outlined in red in (c) and the corresponding EDX elemental mapping. (e) A magnified image of the section outlined in red in (c) and corresponding compositional line profiles. (f) HAADF-STEM images of LFP0.05-RO. The purple circles in (f) mark some of PdO particles. (g) The EDX spectrum measured at position P1 in (f). (h) The EDX spectrum measured at position M1 in (f).

coated TEM copper grid. On the basis of the STEM-EDX analysis, it can be concluded that small nanosized metallic Pd particles appeared on the surface of LFP0.05-R and PdO particles (slightly larger) were formed on the surface of LFP0.05-RO.

X-ray photoelectron spectroscopy (XPS) measurements were performed to analyze the chemical valence states of Pd on the surface of the catalysts. Figure 3 shows the XPS spectra of Pd for LFP0.05, LFP0.05-R, and LFP0.05-RO. As shown, LFP0.05-R exhibited a Pd $3d_{5/2}$ peak at 335.1 eV that unambiguously verified that Pd was in a metallic state (Pd^0).

Additionally, a Pd $3d_{5/2}$ peak at 336.8 eV for LFP0.05-RO clearly indicated that Pd was in the +2 oxidation state (Pd^{2+}). However, LFP0.05 exhibited an unusual Pd $3d_{5/2}$ peak at 337.7 eV, which was higher than the typical value of Pd^{2+} (336.8 eV), suggesting that Pd was in a special ionic environment located in the surface B-site of the perovskite network.[21] There have been debates about whether the valence state of Pd in the perovskites exhibits oxidation states of +3 or +4.[21,26−28] Therefore, it is

DOI: 10.1021/acs.chemmater.5b00450
Chem. Mater. 2015, 27, 3048−3054

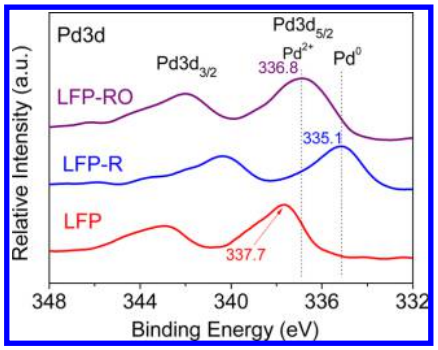

Figure 3. XPS spectra of Pd for the LFP0.05, LFP0.05-R, and LFP0.05-RO catalysts.

reasonable to uniformly regard the state of Pd with high binding energy (BE) in LFP0.05 as perovskite-type ionic (Pi) $Pd^{3/4+}$. Whether the unusual $Pd^{3/4+}$ can occupy the B-site lattice of LF perovskite structure could be predicted using the Goldschmidt tolerance factor, $t = (r_A + r_O)/\sqrt{2}(r_B + r_O)$, where r_A, r_B, and r_O are the ionic radii of the ions (A- and B-sites and oxygen). To form a stable perovskite crystal structure, the tolerance factor t must lie within the range $0.75 < t < 1.0$. Distortion of the BO_6 octahedra happens when the value of t is lower than 1 (for the ideal cubic unit cell). The tolerance factor of LFP0.05 perovskite was determined upon the ionic radii of La^{3+}, Pd^{3+}, Pd^{4+}, and O^{2-} at $r_{La3+} = 1.36$ Å, $r_{Pd3+} = 0.76$ Å, $r_{Pd4+} = 0.62$ Å and $r_{O2-} = 1.40$ Å reported by Shannon et al.[29] and the radius of high spin state of Fe^{3+} at $r_{Fe3+,\,hs} = 0.65$ Å reported by Abbate et al.[30] The obtained tolerance factors of LFP0.05 were 0.949 and 0.953 by assuming all of the Pd ions are in Pd^{3+} and Pd^{4+} in perovskite, respectively, which fall into the range of $0.75 < t < 1.0$. Thus, the unusual 3+ or 4+ oxidation state of Pd could stably be located in the B-site lattice of the perovskite structure. To sum up, our results are in agreement with previous reports of XPS and X-ray absorption near-edge structure (XANES) techniques.[21,31−33] Through the preparation of Pd-containing perovskite and further treatment in reducing and oxidizing atmospheres, we successfully obtained various Pd species with different oxidation states (i.e., LFP0.05-R with Pd^0, LFP0.05-RO with Pd^{2+}, and LFP0.05 with (Pi) $Pd^{3/4+}$). The XPS spectra of Fe for LF, LFP0.05, LFP0.05-R, and LFP0.05-RO were also measured (Figure S1 of the Supporting Information). The BE of the Fe $2p_{3/2}$ peak at 710.8 eV and the Fe $2p_{1/2}$ peak at 724.4 eV confirmed the presence of Fe^{3+} in all of the catalysts. This result indicates that the thermal treatment did not change the valence state of Fe in the LFP0.05 perovskite.[28,33]

Electrochemically Measured ORR Activity of Catalysts. Particle size may affect the ORR activity of the perovskite catalyst. All of the catalysts (including LF, LFP0.05, LFP0.05-R, and LFP0.05-RO) exhibited similar morphologies in which near spherical particles of ∼100 nm in size are observed and these particles agglomerate to form larger chunks (Figure S2 of the Supporting Information), thus excluding their effect on the electrocatalytic activity. To evaluate the effect of the oxidation state of Pd on the ORR catalytic activity, cyclic voltammetry (CV) tests were initially performed on the LFP0.05, LFP0.05-R, and LFP0.05-RO catalysts in an O_2-saturated 0.1 M KOH solution at a scan rate of 100 mV s^{-1}, and the Pd-free LF was also tested to exclude the possible decisive contribution of the $LaFeO_3$ main perovskite matrix to the ORR activity of the three Pd-containing catalysts (Figure 4a). LFP0.05 showed a cathodic peak at −0.41 V, which shifted positively compared with that of LFP0.05-RO (−0.46 V), LFP0.05-R (−0.53 V), and LF (−0.55 V). LFP0.05 also exhibited the highest cathodic peak current

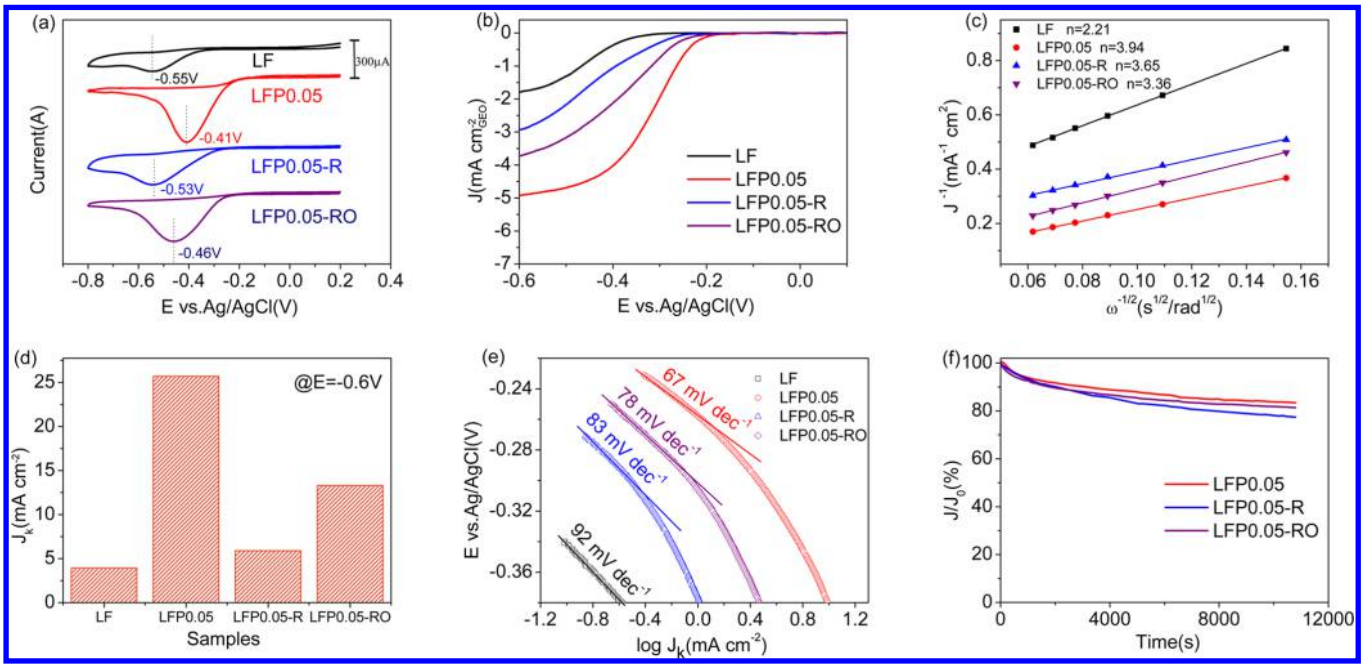

Figure 4. (a) CV curves of LF, LFP0.05, LFP0.05-R, and LFP0.05-RO in an O_2-saturated 0.1 M KOH solution at a scan rate of 100 mV s^{-1}. (b) LSV curves of LF, LFP0.05, LFP0.05-R, and LFP0.05-RO on RDE at 1600 rpm in an O_2-saturated 0.1 M KOH solution at a scan rate of 5 mV s^{-1}. (c and d) The electron transfer number (n) and kinetic-limiting current density (J_k) derived from the K−L plots at −0.6 V for LF, LFP0.05, LFP0.05-R, and LFP0.05-RO on the basis of the RDE data in Figure S4 of the Supporting Information. (e) Tafel plots of LF, LFP0.05, LFP0.05-R, and LFP0.05-RO. (f) Chronoamperometric response of LFP0.05, LFP0.05-R, and LFP0.05-RO at −0.6 V on RDE at 1600 rpm in an O_2-saturated 0.1 M KOH solution.

DOI: 10.1021/acs.chemmater.5b00450
Chem. Mater. 2015, 27, 3048−3054

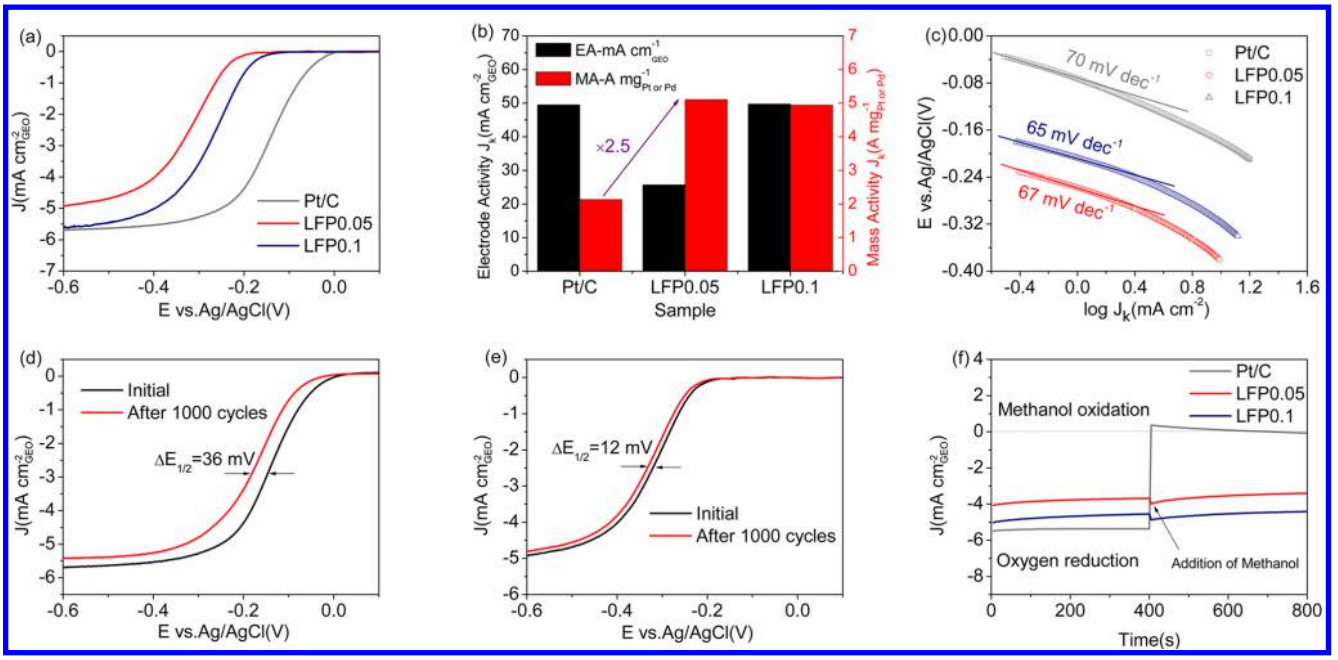

Figure 5. (a) LSV curves of LFP0.05, LFP0.1, and commercial 20 wt % Pt/C on RDE at 1600 rpm in an O_2-saturated 0.1 M KOH solution at a scan rate of 5 mV s^{-1}. (b) ORR electrode activity (EA) and mass activity (MA) of LFP0.05, LFP0.1, and commercial 20 wt % Pt/C at −0.6 V. (c) Tafel plots of LFP0.05, LFP0.1, and commercial 20 wt % Pt/C. (d and e) LSV curves of commercial 20 wt % Pt/C and LFP0.05 at 1600 rpm in an O_2-saturated 0.1 M KOH solution at a scan rate of 5 mV s^{-1} before and after the potential cycling stability test. The potential cycling was performed in an O_2-saturated 0.1 M KOH solution at a scan rate of 100 mV s^{-1} between 0.2 and −0.6 V for 1000 cycles. (f) Chronoamperometric response of LFP0.05, LFP0.1, and commercial 20 wt % Pt/C at −0.4 V in an O_2-saturated 0.1 M KOH solution without methanol (0−400 s) and with the addition of 0.5 M methanol (400−800 s) on RDE at 1600 rpm.

among all of the catalysts, while LF had the lowest value. This result demonstrates that the difference in ORR activity of the three Pd-containing catalysts should be primarily related to the different oxidation states of the Pd element. The more positive peak potential and the higher peak current of LFP0.05 suggest a better electrocatalytic activity for ORR. Similar trends were also observed in rotating-disk electrode (RDE) tests. Figure 4b shows the linear sweep voltammetry (LSV) curves of the LF, LFP0.05, LFP0.05-R, and LFP0.05-RO catalysts on RDE at 1600 rpm in an O_2-saturated 0.1 M KOH solution at a scan rate of 5 mV s^{-1}. LFP0.05 had a more positive half-wave potential ($E_{1/2}$ = −0.32 V) and higher limiting current density (J_L = 4.92 mA cm^{-2}) than LFP0.05-RO (−0.38 V, 3.73 mA cm^{-2}), LFP0.05-R (−0.44 V, 2.93 mA cm^{-2}), and LF (−0.46 V, 1.80 mA cm^{-2}). Notably, to eliminate the effect of the small amounts of impurity phases (~5 wt % $La_2O_3/La(OH)_3$) in the catalysts (e.g., LFP0.05-R or LFP0.05-RO) on the ORR activity, we also prepared LFP0.05 containing 5 wt % $La_2O_3/La(OH)_3$ via physical mixing and infiltration methods and compared their activity (Figure S3 of the Supporting Information). The LSV curves of LFP0.05 containing 5 wt % $La_2O_3/La(OH)_3$ via two methods were nearly identical to that of pristine LFP0.05, suggesting that small amounts of impurity phases in the catalysts had a negligible effect on the ORR activity.

For further insight into the ORR kinetics and electrocatalytic processes on the catalyst, we carried out a more detailed study of the RDE experiments at different rotation speeds (400−2500 rpm, Figure S4 of the Supporting Information). As calculated from the slope of the Koutecky−Levich (K−L) plots (Figure 4c), the electron transfer number (n) at −0.6 V is 2.21, 3.94, 3.65, and 3.36 for LF, LFP0.05, LFP0.05-R, and LFP0.05-RO, respectively. This result suggests a dominant $4e^-$ ORR process for the LFP0.05, LFP0.05-R, and LFP0.05-RO catalysts, while a dominant $2e^-$ ORR process for the LF catalyst. This result also indicates that the Pd had intrinsically better activity than LF perovskite for ORR. Furthermore, the ORR activity of the catalysts can be reflected by the kinetic-limiting current density (J_k). As shown in Figure 4d, the J_k values of the catalysts at −0.6 V follow the order, in the sequence of LFP0.05 (25.69 mA cm^{-2}) > LFP0.05-RO (13.29 mA cm^{-2}) > LFP0.05-R (5.88 mA cm^{-2}) > LF (3.92 mA cm^{-2}). To gain more information on the kinetics of ORR, Tafel plots of these catalysts were also drawn in Figure 4e. The Tafel slopes are 92, 67, 83, and 78 mV dec^{-1} for LF, LFP0.05, LFP0.05-R, and LFP0.05-RO, respectively. LFP0.05 exhibited the smallest Tafel slope, rigidly proving its excellent charge-transfer rate (Figure S5 of the Supporting Information) and is therefore the most efficient electrocatalyst with the fastest ORR kinetics. In addition to the activity, the durability is another important parameter for ORR catalysts. The durability of the LFP0.05, LFP0.05-R, and LFP0.05-RO catalysts was evaluated by the chronoamperometric response under a constant cathodic voltage of −0.6 V, as shown in Figure 4f. LFP0.05 exhibited better stability than LFP0.05-R and LFP0.05-RO, and it is likely that the Pd in LFP0.05 was fixed in the perovskite lattice, thus avoiding the grain growth that might be experienced by LFP0.05-R and LFP0.05-RO samples. Therefore, according to the above electrochemical analysis (with the results summarized in Table S1 of the Supporting Information), increasing the oxidation state of Pd effectively enhanced the ORR activity (i.e., in the order of Pd^0 < Pd^{2+} < perovskite-type ionic (Pi) $Pd^{3/4+}$).

Comparison of ORR Performance between LFP and Pt/C. On the basis of the above results, LFP0.05 with Pi $Pd^{3/4+}$ exhibited the best ORR performance. Besides, Pt/C has been recognized as a benchmark catalyst with the most efficient catalytic activity for ORR. Accordingly, it is meaningful to

DOI: 10.1021/acs.chemmater.5b00450
Chem. Mater. 2015, 27, 3048−3054

compare their ORR performance. The LSV curves in Figure 5a revealed that LFP0.05 still maintained lower ORR electrode activity (based on the glassy carbon area) than the commercial 20 wt % Pt/C (as characterized by TEM and shown in Figure S6 of the Supporting Information) in terms of half-wave potential and the limiting current density. Notably, when we increased the content of Pd from 2.17% (molar mass fraction) in LFP0.05 to 4.34% in LFP0.1 (characterized by XRD and XPS shown in Figures S7 and S8 of the Supporting Information), the ORR electrode activity was further enhanced. The limiting current density of LFP0.1 could reach that of Pt/C, although a negative shift existed in the half-wave potential of LFP0.1 compared with Pt/C. Here, it should be noted that the limiting current density and half-wave potential values of the commercial 20 wt % Pt/C in our work are in good agreement with other literature reports with similar electrode preparation and loading.[34−37] Considering the cost of the catalysts and the economic feasibility, the electrode activity (EA) with the kinetic-limiting current density (J_k) constructed from a rotation rate-dependent current density (Figures S4b and S9 of the Supporting Information) based on the glassy carbon area and mass activity (MA) with J_k based on the Pt or Pd mass of the tested catalysts were calculated and shown in Figure 5b. The EA of LFP0.05 was 25.69 mA cm^{-2}, which was lower than that of Pt/C (49.48 mA cm^{-2}). However, LFP0.1 containing a higher content of Pi $Pd^{3/4+}$ delivered a comparable EA (49.75 mA cm^{-2}) to Pt/C. If taking the noble metal mass into account solely, the MA of LFP0.05 is 5.12 A mg_{Pd}^{-1}, which was similar to that of LFP0.1 (4.96 A mg_{Pd}^{-1}) and ∼2.5 times higher than that of Pt/C (2.13 A mg_{Pt}^{-1}). The intrinsic activity, namely, the turnover frequency (TOF) per active site (Pd or Pt), excluding the contribution from the LF main perovskite matrix, is another key factor governing the ORR activity of the catalysts. LFP0.05 and LFP0.1 catalyzed the ORR with a TOF ∼ 5-fold higher than the Pt/C catalyst and ∼84-fold higher than the LFP0.05-R (Figure S10 of the Supporting Information). Additionally, the superior ORR performance of LFP0.05 and LFP0.1 was also indicated by the Tafel plots (Figure 5c). The Tafel slopes are 67, 65, and 70 mV dec^{-1} for LFP0.05, LFP0.1 and Pt/C, respectively. The smaller Tafel slope of LFP than Pt/C is an indication of faster ORR kinetics.

The cycle stability is another critical performance metric that determines the practicability of electrocatalysts. To assess this, the accelerated stability tests of the LFP and Pt/C catalysts were conducted by potential cycling between 0.2 and −0.6 V at a scan rate of 100 mV s^{-1} in an O_2-saturated 0.1 M KOH solution. As shown in Figure 5 (panels d and e) and Figure S11 of the Supporting Information, only a slight change in the half-wave potential (∼12 mV for LFP0.05 and ∼9 mV for LFP0.1) was observed even after 1000 continuous potential cycles, while there was ∼36 mV loss of half-wave potential for Pt/C, suggesting the superior durability of the LFP catalysts. It could be ascribed to the stable $Pd^{3/4+}$ oxidation states in the B-site lattice of the perovskite network. In addition to the significance of stability, the methanol tolerance ability is also an important issue for cathode materials in certain low-temperature fuel cells (e.g., direct methanol fuel cells). Remarkably, as shown in Figure 5f, the original cathodic ORR current of LFP0.05 and LFP0.1 under −0.4 V exhibited only a slight change after the introduction of 0.5 M methanol. In contrast, the corresponding current of Pt/C shifted from a cathodic current to a reversed anodic current in a short time after the addition of methanol, indicating a conversion of the dominant ORR to the methanol oxidation reaction (i.e., methanol poisoning effects). The same phenomenon was also reflected by the LSV curves after the addition of methanol (Figure S12 of the Supporting Information). These results indicated that LFP also had a significantly better tolerance to the methanol crossover effect than commercial Pt/C and can be an ideal cathode catalyst for direct methanol fuel cells.

Nature of Oxidation State-Dependent ORR Activity for Pd. To elucidate the nature of the different ORR activities of the Pd catalysts with different oxidation states (following the order of Pi $Pd^{3/4+}$ > Pd^{2+}> Pd^0), we first proposed a possible explanation from molecular orbital principles. Suntivich et al. have reported a volcano plot showing a correlation between the ORR activity and the e_g filling of different perovskites.[20] They found that perovskites containing transition metals with an e_g = 1 filling have the highest ORR activity in the alkaline solution.[20] We believe the descriptor can also be applied to the noble metal (e.g., Pd). This conjecture is supported by the correlation between the increased e_g filling (Figure S13 of the Supporting Information) and decreased ORR activity in the order of Pi $Pd^{3/4+}$ (e_g = 1, which is based on previous related literature data[26,38]) > Pd^{2+} (e_g = 2) > Pd^0 (e_g = 4). Another possible origin of the enhanced ORR activity with the increase in the oxidation states of Pd is related to the d-band center. Normally, there are three general intermediate steps in the entire ORR: the adsorption of O_2, the reduction of O_2, and the removal of the generated OH. Recently, both theoretical calculations and experimental results have shown that oxygen binds more strongly on Pd than on Pt; thus, the rate-determining step (RDS) on Pd for ORR is the removal of the generated OH species.[39−41] Furthermore, previous studies have also found that a decrease in electron density (d-band center) with the generation of a weaker Pd−O band could decrease the superficial coverage by the generated OH, leading to the release of more active sites for O_2 adsorption.[16,19,39,42] From the above XPS characterization, the binding energy of Pd 3d shifted more positively as the valence state of Pd increased. The positive shift could thereby decrease the electron density (downshift of the d-band center) in Pd (Figure S14 of the Supporting Information), causing the Pd surface to be easily accessible for O_2 adsorption and activation, and thus improving the ORR activity.[16,19] Some modeling methods [e.g., density functional theory (DFT) calculations] are required to confirm this in our future work. Besides the above-mentioned origins, other ones are also possible; future in-depth investigation could shed more light on this.

4. CONCLUSIONS

In summary, we synthesized various Pd catalysts with different oxidation states through a novel and simple approach based on the reduction−oxidation treatment of LFP0.05 and compared their ORR activities. The order of Pd^0 < Pd^{2+} < Pi $Pd^{3/4+}$ was demonstrated, and the intrinsic activity of (Pi) $Pd^{3/4+}$ was ∼84-fold higher than that of Pd^0. Particularly, the LFP perovskite (containing Pi $Pd^{3/4+}$ with the highest ORR activity among the various valence states) exhibited a higher mass activity, better durability, and higher tolerance to methanol than the benchmark commercial Pt/C catalyst. The superior ORR performance of Pi $Pd^{3/4+}$ may possibly be ascribed to the optimal e_g orbital filling (e_g = 1) and the downshift of the d-band center. This finding highlights the importance of tuning the noble metal Pd to the perovskite-type ionic Pd state as a promising strategy for the optimal use of Pd for catalyzing

DOI: 10.1021/acs.chemmater.5b00450
Chem. Mater. 2015, 27, 3048−3054

ORR. Moreover, considering the universality of the method, we believe the strategy presented in this study to optimize Pd can also be extended to the development of various other noble metal (e.g., Pt, Ru, and Rh)-containing perovskites with expected capabilities for various applications, such as fuel cells, metal-air batteries, supercapacitors and sensors, among others.

■ ASSOCIATED CONTENT

Supporting Information

XPS spectra of Fe, SEM images with different magnifications, XRD profiles and LSV curves, electrochemical impedance spectra, TEM image of commercial 20 wt % Pt/C, XRD profiles, XPS spectra of LFP0.1, turnover frequency, schematic representation of e_g, schmatic representation of Pd, and summary of some electrochemical parameters reflecting ORR activity. This material is available free of charge via the Internet at http://pubs.acs.org.

■ AUTHOR INFORMATION

Corresponding Authors

*E-mail: zhouwei1982@njtech.edu.cn.
*E-mail: shaozp@njtech.edu.cn.

Notes

The authors declare no competing financial interest.

■ ACKNOWLEDGMENTS

This work was financially supported by the Key Projects in Nature Science Foundation of Jiangsu Province under contract No. BK2011030 and by the Priority Academic Program Development of Jiangsu Higher Education Institutions and the Program for Jiangsu Specially-Appointed Professors.

■ REFERENCES

(1) Wen, Z.; Ci, S.; Zhang, F.; Feng, X.; Cui, S.; Mao, S.; Luo, S.; He, Z.; Chen, J. *Adv. Mater.* **2012**, *24*, 1399.
(2) Lu, Y. C.; Xu, Z. C.; Gasteiger, H. A.; Chen, S.; Hamad-Schifferli, K.; Shao-Horn, Y. *J. Am. Chem. Soc.* **2010**, *132*, 12170.
(3) Moussallem, I.; Jorissen, J.; Kunz, U.; Pinnow, S.; Turek, T. *J. Appl. Electrochem.* **2008**, *38*, 1177.
(4) Stamenkovic, V. R.; Fowler, B.; Mun, B. S.; Wang, G.; Ross, P. N.; Lucas, C. A.; Marković, N. M. *Science* **2007**, *315*, 493.
(5) Wen, Z.; Wang, Q.; Li, J. *Adv. Funct. Mater.* **2008**, *18*, 959.
(6) Debe, M. K. *Nature* **2012**, *486*, 43.
(7) Arenz, M.; Mayrhofer, K.; Stamenkovic, V.; Blizanac, B.; Tomoyuki, T.; Ross, P.; Markovic, N. *J. Am. Chem. Soc.* **2005**, *127*, 6819.
(8) Liu, H. Q.; Koenigsmann, C.; Adzic, R. R.; Wong, S. S. *ACS Catal.* **2014**, *4*, 2544.
(9) Bianchini, C.; Shen, P. K. *Chem. Rev.* **2009**, *109*, 4183.
(10) Antolini, E. *Energy Environ. Sci.* **2009**, *2*, 915.
(11) Xiao, L.; Zhuang, L.; Liu, Y.; Lu, J.; Abruña, H. D. *J. Am. Chem. Soc.* **2009**, *131*, 602.
(12) Poon, K. C.; Tan, D. C. L.; Vo, T. D. T.; Khezri, B.; Su, H. B.; Webster, R. D.; Sato, H. *J. Am. Chem. Soc.* **2014**, *136*, 5217.
(13) Jiang, L.; Hsu, A.; Chu, D.; Chen, R. *J. Electrochem. Soc.* **2009**, *156*, B643.
(14) Lee, C. L.; Chiou, H. P. *Appl. Catal., B* **2012**, *117*−*118*, 204.
(15) Kondo, S.; Nakamura, M.; Maki, N.; Hoshi, N. *J. Phys. Chem. C* **2009**, *113*, 12625.
(16) Liu, Y. Q.; Xu, C. X. *ChemSusChem* **2013**, *6*, 78.
(17) Qi, Y.; Wu, J. B.; Zhang, H.; Jiang, Y. Y.; Jin, C. H.; Fu, M. S.; Yang, H.; Yang, D. R. *Nanoscale* **2014**, *6*, 7012.
(18) Toyoda, E.; Jinnouchi, R.; Ohsuna, T.; Hatanaka, T.; Aizawa, T.; Otani, S.; Kido, Y.; Morimoto, Y. *Angew. Chem., Int. Ed.* **2013**, *52*, 4137.
(19) Lu, Y. Z.; Jiang, Y. Y.; Gao, X. H.; Wang, X. D.; Chen, W. *J. Am. Chem. Soc.* **2014**, *136*, 11687.
(20) Suntivich, J.; Gasteiger, H. A.; Yabuuchi, N.; Nakanishi, H.; Goodenough, J. B.; Shao-Horn, Y. *Nat. Chem.* **2011**, *3*, 546.
(21) Uenishi, M.; Taniguchi, M.; Tanaka, H.; Kimura, M.; Nishihata, Y.; Mizuki, J.; Kobayashi, T. *Appl. Catal., B* **2005**, *57*, 267.
(22) Shao, Z. P.; Haile, S. *Nature* **2004**, *431*, 170.
(23) Taguchia, H.; Masunagab, Y.; Hirotab, K.; Yamaguchi, O. *Mater. Res. Bull.* **2005**, *40*, 773.
(24) Eyssler, A.; Winkler, A.; Sofonova, O.; Nachtegaal, M.; Matam, S. K.; Hug, P.; Weidenkaff, A.; Ferri, D. *Chem. Mater.* **2012**, *24*, 1864.
(25) Uenishi, M.; Tanaka, H.; Taniguchi, M.; Tan, I.; Sakamoto, Y.; Matsunaga, S.; Yokota, K.; Kobayashi, T. *Appl. Catal., A* **2005**, *296*, 114.
(26) Nishihata, Y.; Mizuki, J.; Akao, T.; Tanaka, H.; Uenishi, M.; Kimura, M.; Okamoto, T.; Hamadak, N. *Nature* **2002**, *418*, 164.
(27) Misch, L. M.; Birkel, A.; Figg, C. A.; Fors, B. P.; Hawker, C. J.; Stucky, G. D.; Seshadri, R. *Dalton Trans.* **2014**, *43*, 2079.
(28) Giraudon, J.-M.; Elhachimi, A.; Leclercq, G. *Appl. Catal., B* **2008**, *84*, 251.
(29) Shannon, R. D.; Prewitt, C. T. *Acta Crystallogr.* **1969**, *B25*, 925.
(30) Abbate, M.; deGroot, F. M. F.; Fuggle, J. C.; Fujimori, A.; Strebel, O.; Lopez, F.; Domke, M.; Kaindl, G.; Sawatzky, G. A.; Takano, M.; Takeda, Y.; Eisaki, H.; Uchida, S. *Phys. Rev. B* **1992**, *46*, 4511.
(31) Tanaka, H.; Tan, I.; Uenishi, M.; Taniguchi, M.; Kimura, M.; Nishihata, Y.; Mizuki, J. *J. Alloys Compd.* **2006**, *408*−*412*, 1071.
(32) Eyssler, A.; Mandaliev, P.; Winkler, A.; Hug, P.; Safonova, O.; Figi, R.; Weidenkaff, A.; Ferri, D. *J. Phys. Chem. C* **2010**, *114*, 4584.
(33) Nishihata, Y.; Mizuki, J.; Tanaka, H.; Uenishi, M.; Kimura, M. *J. Phys. Chem. Solids* **2005**, *66*, 274.
(34) Li, Y. G.; Zhou, W.; Wang, H. L.; Xie, L. M.; Liang, Y. Y.; Wei, F.; Idrobo, J.-C.; Pennycook, S. J.; Dai, H. J. *Nat. Nanotechnol.* **2012**, *7*, 394.
(35) Bian, W. Y.; Yang, Z. R.; Strasser, P.; Yang, R. Z. *J. Power Sources* **2014**, *250*, 196.
(36) Liang, Y. Y.; Li, Y. G.; Wang, H. L.; Zhou, J. G.; Wang, J.; Regier, T.; Dai, H. J. *Nat. Mater.* **2011**, *10*, 780.
(37) Yang, W.; Fellinger, T.-P.; Antonietti, M. *J. Am. Chem. Soc.* **2011**, *133*, 206.
(38) Hamada, I.; Uozumi, A.; Morikawa, Y.; Yanase, A.; Katayama-Yoshida, H. *J. Am. Chem. Soc.* **2011**, *133*, 18506.
(39) Suo, Y. G.; Zhuang, L.; Lu, J. T. *Angew. Chem., Int. Ed.* **2007**, *46*, 2862.
(40) Yang, L. J.; Vukmirovic, M. B.; Su, D.; Sasaki, K.; Herron, J. A.; Mavrikakis, M.; Liao, S. J.; Adzic, R. R. *J. Phys. Chem. C* **2007**, *111*, 404.
(41) Seo, M. H.; Choi, S. M.; Seo, J. K.; Noh, S. H.; Kim, W. B.; Han, B. *Appl. Catal., B* **2013**, *129*, 163.
(42) Mukerjee, S.; Srinivasan, S.; Soriaga, M. P.; McBreen, J. *J. Electrochem. Soc.* **1995**, *142*, 1409.

DOI: 10.1021/acs.chemmater.5b00450
Chem. Mater. 2015, 27, 3048−3054